

Enhanced Electronic Transport in Disordered Hyperuniform Two-Dimensional Amorphous Silica

Yu Zheng*,¹ Lei Liu*,² Hanqing Nan*,² Zhen-Xiong Shen*,^{3,4} Ge Zhang,⁵ Duyu Chen,⁶ Lixin He,^{3,4} Wenxiang Xu,^{7,2,†} Mohan Chen,^{8,‡} Yang Jiao,^{2,1,§} and Houlong Zhuang^{2,¶}

¹*Department of Physics, Arizona State University, Tempe, AZ 85287*

²*Materials Science and Engineering, Arizona State University, Tempe, AZ 85287*

³*Key Laboratory of Quantum Information, University of Science and Technology of China, Hefei, Anhui 230026, P. R. China*

⁴*Synergetic Innovation Center of Quantum Information and Quantum Physics, University of Science and Technology of China, Hefei, Anhui 230026, P. R. China*

⁵*Department of Physics, University of Pennsylvania, Philadelphia, PA 19104*

⁶*Tepper School of Business, Carnegie Mellon University, Pittsburgh, PA 15213*

⁷*College of Mechanics and Materials, Hohai University, Nanjing 211100, P.R. China*

⁸*CAPT, HEDPS, College of Engineering, Peking University 100871, P.R. China*

Disordered hyperuniformity (DHU) is a recently proposed new state of matter, which has been observed in a variety of classical and quantum many-body systems. DHU systems are characterized by vanishing infinite-wavelength density fluctuations and are endowed with unique novel physical properties. Here we report the first discovery of disordered hyperuniformity in atomic-scale 2D materials, i.e., amorphous silica composed of a single layer of atoms, based on spectral-density analysis of high-resolution transmission electron microscope images. Subsequent simulations suggest that the observed DHU is closely related to the strong topological and geometrical constraints induced by the local chemical order in the system. Moreover, we show via large-scale density functional theory calculations that DHU leads to almost complete closure of the electronic band gap compared to the crystalline counterpart, making the material effectively a metal. This is in contrast to the conventional wisdom that disorder generally diminishes electronic transport and is due to the unique electron wave localization induced by the topological defects in the DHU state.

Disorder hyperuniform (DHU) systems are a unique class of disordered systems which suppress large-scale density fluctuations like crystals and yet possess no Bragg peaks [1, 2]. For a point configuration (e.g., a collection of particle centers of a many-body system), hyperuniformity is manifested as the vanishing structure factor in the infinite-wavelength (or zero-wavenumber) limit, i.e., $\lim_{k \rightarrow 0} S(k) = 0$, where $k = 2\pi/\lambda$ is the wavenumber. In this case of a random field, the hyperuniform condition is given by $\lim_{k \rightarrow 0} \hat{\psi}(k) = 0$, where $\hat{\psi}(k)$ is the spectral density [2]. It has been suggested that hyperuniformity can be considered as a new state of matter [1], which possesses a hidden order in between of that of a perfect crystal and a totally disordered system (e.g. a Poisson distribution of points).

Recently, a wide spectrum of physical and biological systems have been identified to possess the remarkable property of hyperuniformity, which include the density fluctuations in early universe [3], disordered jammed packing of hard particles [4–7], certain exotic classical ground states of many-particle systems [8–15], jammed colloidal systems [16–19], driven non-equilibrium systems [20–23], certain quantum ground states [24, 25], avian photoreceptor patterns [26], organization of adapted im-

mune systems [27], amorphous silicon [28, 29], a wide class of disordered cellular materials [30], dynamic random organizing systems [31–35], and even the distribution of primes on the number axis [36]. In addition, it has been shown that hyperuniform materials can be designed to possess superior physical properties including large isotropic photonic band gaps [37–39], optimized transport properties [40], mechanical properties [41] as well as optimal multi-functionalities [42]. Designer DHU materials have also been successfully fabricated or synthesized using different techniques [43, 44].

In this letter, we report the discovery of hyperuniformity in amorphous 2D silica (conventionally modeled as “continuous random networks” [45]), based on the analysis of aberration corrected transmission electron microscopy (TEM) images of the material. To the best of our knowledge, this is the first discovery of disordered hyperuniformity in atomic scale 2D materials (i.e., those composed of a single layer of atoms), which can possess unique novel electronic, magnetic and optical properties compared to their bulk counterparts.

We show via simulations that the observed DHU in amorphous silica is closely related to the strong topological and geometrical constraints induced by the local chemical order in the system. In addition, our density functional theory calculations show that DHU significantly reduces the electronic band gap in 2D amorphous silica, leading to almost complete closure of the band gap compared to the crystalline counterpart. This is in contrast to the conventional wisdom that disorder generally diminishes electronic transport and is due to the unique

*These authors contributed equally to this work.

†correspondence sent to: xwxfat@gmail.com

‡correspondence sent to: mohanchen@pku.edu.cn

§correspondence sent to: yang.jiao.2@asu.edu

¶correspondence sent to: hzhuang7@asu.edu

electron wave localization induced by DHU.

Hyperuniformity in 2D amorphous silica. We first analyze the high-resolution transmission electron microscopy (TEM) images of 2D amorphous silica, see Fig.1a. The materials samples were fabricated using chemical vapor deposition (CVD) and the procedure for obtaining the imaging data set was reported in detail in Ref. [46] and briefly described in the Supporting Information (SI). As shown in Fig. 1a, the black spots (with diffusive boundaries) represent the silicon atoms. The micrographs are processed to retain the distribution information of the silicon atoms by thresholding and fitting the grayness intensity distribution associated with each silicon atom using a Gaussian function, i.e., $G(\mathbf{x}) = I_0 e^{-|\mathbf{x}-\mathbf{x}_i|^2/\sigma^2}$, where I_0 is the maximal intensity, \mathbf{x}_i is the center of the silicon atom and σ is an effective radius.

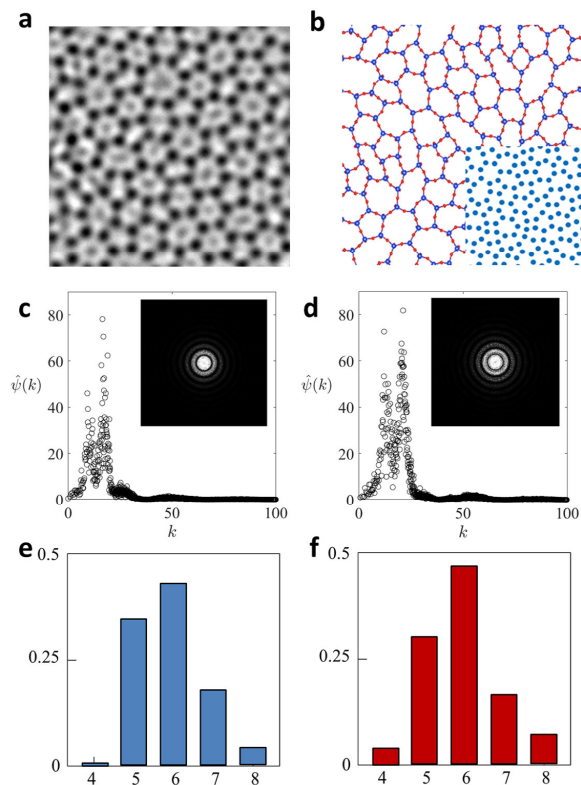


FIG. 1: Hyperuniformity in 2D amorphous silica. (a) TEM image of 2D amorphous silica. Reproduced from Ref. [46] (b) Disordered hyperuniform silica network generated via computer simulations as described in the text. Blue and red spheres denote Si and O atoms, respectively. Inset shows intensity map derived from the positions of silicon atoms for spectral density analysis. (c) and (d) respectively show the angularly averaged spectral density $\psi(\mathbf{k})$ associated with the TEM micrograph and the simulated amorphous silica network. Insets show the full spectral density. (e) and (f) respectively show the local “ring” statistics of the experimentally obtained and simulated 2D amorphous silica network.

The associated spectral density $\hat{\psi}(\mathbf{k})$ (where \mathbf{k} is the

wave-vector) is computed following Ref. [47] and shown in the inset of Fig.1c. The angularly averaged $\hat{\psi}(k)$ (with $k = |\mathbf{k}|$) is shown Fig.1c. We note that the spectral density analysis (instead of structure factor) is employed here to efficiently utilize all of the information on Si atom distributions contained in the TEM micrographs and minimize the possible systematic errors induced by converting the intensity map into center distributions. It can be seen that $\hat{\psi}(\mathbf{k})$ is fully isotropic and the scattering is completely suppressed at infinite wavelength, i.e., $\lim_{k \rightarrow 0} \hat{\psi}(k) = 0$ with $\hat{\psi}(k) \sim k$ for small k values, which indicates that the 2D amorphous silica samples analyzed are hyperuniform (see SI for detailed scaling analysis).

Next, we computationally generate disordered hyperuniform silica networks. We note that unlike 3D amorphous materials such as metallic glasses which can be simulated by numerically quenching a high temperature liquid state, even very rapid quenching of a 2D materials will lead to a highly crystalline materials with a small number of local defects. Such defected crystalline materials clearly cannot represent the experimentally obtained DHU amorphous silicon. Together with the observation that the 2D silica systems are HU, this motivates us to employ a structure-based method, which is a two-step approach.

In the first step, a three-coordinated DHU network is generated using a modified “collective coordinate” approach [11], in which a random initial configuration of points is gradually evolved to match a prescribed targeted structure factor $S^*(k)$ while simultaneously satisfying mutual exclusion volume constraints. The targeted $S^*(k) = 0$ for $k \leq K^*$ drives the system to a hyperuniform state and the exclusion volume constraints ensure the final configuration can be feasibly mapped to an amorphous silica network. In the second step, the obtained point configuration is mapped to a three-coordinated network by connecting a point with its three nearest neighbors. This network is further converted to a silica network, by placing a silicon atom centered at each point and placing an oxygen atom at the mid-point of the two connected silicon atoms. We then perform molecular statics simulations using the Si-O potential based on the Tersoff parameterization [48] as implemented in the LAMMPS program [49] to optimize the constructed silica network to physically metastable states by minimizing their total potential energy.

The spectral density of the simulated amorphous silica network (see Fig.1b) is computed by placing a Gaussian kernel function at the center of each silicon atom and is shown in Fig.1d. It can be clearly seen that $\hat{\psi}(k)$ of the simulated network agrees very well with the experimental data for all wave numbers including the zero- k limit, i.e., $\lim_{k \rightarrow 0} \hat{\psi}(k) = 0$ with $\hat{\psi}(k) \sim k$ for small k values (see SI for detailed scaling analysis and comparison to experimental results).

We note that in the second step of the simulation (i.e., the potential energy minimization), hyperuniformity (i.e., the small k values of $S(k)$) is not constrained

anymore. The evolution of the system is dominated by the interactions of atoms and constrained by the topology, and the positions of the atoms have been significantly perturbed compared to the final configuration obtained in the first step. Yet the resulting system is still hyperuniform. This result suggests the strong geometrical and topological constraints, i.e., the bond length and angle associated with the Si-O bonds as well as 3-coordinated configurations, induced by the local chemical order could lead to the observed hyperuniformity in the system.

We also obtain and compare the number of n -fold rings (where $n = 3, 4, \dots$) formed by silicon atoms in both the experimental and simulated networks, see Fig.1(e) and 1(f). The ring statistics for the two systems again agree very well with one another. In addition, the comparison of local structural statistics of the experimental and numerical systems, including the pair correlation function and nearest neighbor distribution of the Si atoms also show excellent agreement (see SI for details). These results indicate our numerical network model can provide a statistically accurate structural representation of the 2D amorphous silica system by capturing key correlations on both large and small length scales as well as the local topological order. Therefore, we expect that the physical properties computed based on the numerical network model should also be representative of those of the experimental system.

What is the origin of DHU in 2D amorphous silica? We note that as a first approximation, the 2D silica glass can be considered as obtained from a 2D crystalline silica network by continuously introducing the Stone-Wales (SW) defects [50], which change the topology of the network. However, the SW defects do not affect the number of particles within a large observation window, since the SW transformation is localized and only affects a pair of atoms on the single-bond scale. Nonetheless, SW transformations of atom pairs on the boundary of the observation window might lead to a bounded fluctuation of particle numbers, which are scaled with the surface area of the window. Therefore, the SW defects should preserve hyperuniformity in the system. We provide numerical evidence for this speculation in the SI. Although the actual 2D amorphous silica possesses a structure that deviates from the ideal SW transferred crystalline network, the above argument could provide a possible explanation of the observed DHU in the system.

Disordered hyperuniformity significantly reduces electronic band gap. We use the simulated DHU SiO_2 networks to calculate its density of states (DOS) at the DFT-PBE [51] level of theory. Specifically, the DHU structure consists of three sublayers (1800 atoms; 600 Si atoms and 1200 O atoms). For comparison, we also create a supercell of 2D crystalline SiO_2 with the same number of Si and O atoms. Several models of 2D crystalline SiO_2 have been studied using DFT calculations in the literature [52]. Here we refer 2D crystalline SiO_2 to the hexagonal bilayer crystalline network

observed in experiment [53].

We use numerical atomic orbitals [54] as implemented in the ABACUS package [55] for calculating the electronic structure. The simulation methods and parameters can be found in Ref. [56]. For comparison, we also compute the DOS for 2D hexagonal crystalline SiO_2 . The energy difference between the 2D DHU and hexagonal crystalline SiO_2 calculated from the Tersoff potential and DFT are both positive and comparable (0.074 and 0.134 eV/atom, respectively). The positive energy differences indicate that the crystalline structure is more energetically stable than the DHU structure. Nevertheless, the TEM image (see Fig.1(a)) shows that the experimental atomic structure of 2D amorphous SiO_2 is drastically different from the crystalline model. By contrast, the high similarity between the DHU model and experimentally observed atomic structure reveals the metastable nature of DHU systems.

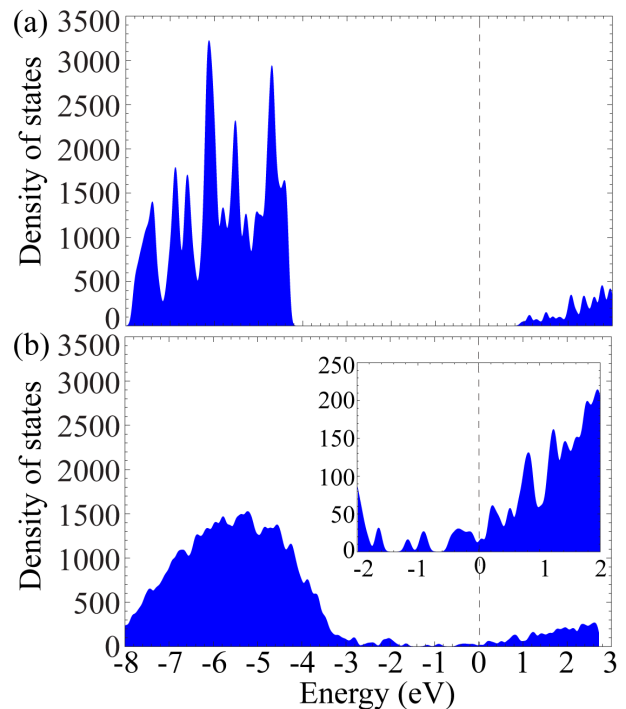


FIG. 2: Density of states of the supercells of 2D (a) crystalline and (b) hyperuniform SiO_2 calculated using density functional theory. The inset shows a zoom-in view of the DOS near the Fermi level.

Figure 2 (a) shows that the 2D crystalline SiO_2 is essentially an insulator with a predicted band gap of 5.31 eV, consistent with the previously reported band gap of 5.48 eV calculated for a unit cell at the same level of theory [57]. By contrast, we observe from Fig. 2(b) that a small but finite number of states occupy the Fermi level of the DHU structure, showing *metallic* behavior of the electrons with a typical band gap of ~ 50 meV. This is comparable to the thermal fluctuations at room temperature ~ 25 meV. In other words, the disordered hyperuniformity fundamentally changes the electrical transport

behavior of 2D SiO₂, from an effective insulator at room temperature (as in the crystalline form) to an effective metal (as in the DHU form).

From Fig. 2(b), we estimate the density ρ of the electrons that contribute to the electrical conductivity of the DHU structure at room temperature. By integrating the number of states in the energies ranging from 25 meV (corresponding to the thermal energy) to the Fermi level in Fig. 2(b), we determine ρ as $2.33 \times 10^{12} \text{ cm}^{-2}$. This magnitude belongs to the category of “high doping” (e.g., 6.0×10^{11} and $9.2 \times 10^{12} \text{ cm}^{-2}$) applied to common 2D semiconductors such as WS₂ and MoS₂ [58]. To put it another way, considering the electron density alone, the conductivity associated with the DHU structure could be comparable to those of the 2D materials.

To better understand this metallic behavior of DHU 2D SiO₂, we compute the charge densities within an energy window of 0.5 eV below the highest occupied molecular orbital (HOMO) level for the crystalline structure and below the Fermi level for the DHU structure. For the former structure, Fig.3(a) (a complete version of Fig.3 can be found in the supplemental material) shows that the electrons are distributed around Si and O atoms in the entire structure, i.e., fully occupying the valence bands. The amount of these electrons is significant, as can be seen from the large DOS below the HOMO level. But these electrons cannot be thermally excited at room temperature to the conduction bands due to the large band gap, leading to zero electrical conductivity for pure 2D crystalline SiO₂.

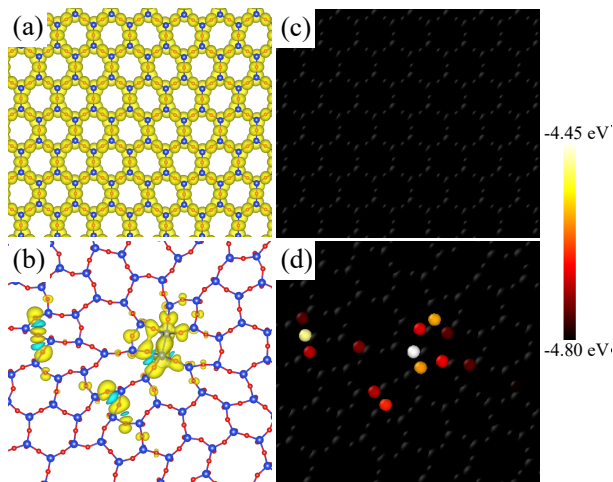


FIG. 3: Electron densities at the HOMO level of (a) the crystalline structure and (b) at the Fermi level of the DHU structure. The isosurface values is $0.0023 e/\text{Bohr}^3$. The corresponding distributions of potential energies are shown in (c) and (d), respectively. The color bar shows a range of the distributions.

On the other hand, for the DHU structure, the number of valence electrons in the same energy window is much less, resulting in a low carrier density but nevertheless, a non-zero conductivity. A closer look at the slightly wider

energy window associated with lowest density of states (e.g., $-2\sim 0$ eV) reveals that the distribution of states still forms an almost continuous spectrum of peaks, see the inset in Fig. 2(b). Figure 3(b) reveals that the valence electrons contributing to the conductivity originate from a small portion of the Si and O atoms in the DHU system.

Topological defects in DHU SiO₂ lead to electron localization with high energies. To understand why the electrons are localized around these atoms, we show in Fig. 3(c) and 3(d) the distributions of the computed potential energies using the Tersoff potential for the crystalline and DHU systems, respectively. Consistent with Fig. 3(a), Fig. 3(c) shows that the potential energies are homogeneously distributed in the crystalline system. On the contrary, for the DHU system, we observe from Fig. 3(d) that the potential energies possess a highly heterogeneous distribution, with significantly higher energies localized in regions where the atomic arrangements significantly deviates from the 6-fold hexagonal configuration. These are topological defects which are necessary to achieve DHU in amorphous 2D silica. Importantly, the high-energy localizations perfectly coincide with the electron localizations (see Figure 3(b)), indicating that the local potential energies due to the topological defects induced by DHU are sufficiently high to activate the electrons to the energy levels near the Fermi energy.

Electron localization in a disordered system is generally associated with a number of exotic physical phenomena [59] such as metal-to-insulator transitions suggested by Anderson [60]. The electron localization in the DHU silica system appears to be phenomenologically different from the Anderson localization, as the DHU localization gives rise the opposite (i.e., insulator-to-metal) transition. A mathematical model based on model Hamiltonian that considers the disordered potential needs to be devised in order to investigate the electrical transport property of the localized electrons. Furthermore, whether the insulator-to-metal transition also occurs in other 2D DHU semiconductors/insulators remains unknown and is certainly worth exploring.

In summary, we have discovered, for the first time, disordered hyperuniformity in 2D amorphous materials, and showed that DHU fundamentally changes the electronic transport behaviors in the material, making 2D DHU silica metallic. This interesting prediction clearly awaits for experimental confirmation. We also showed that the metallic behavior (i.e., with a virtually continuous spectrum of DOS without significant band gaps in DHU silica) is resulted from the localization of high-energy states due to the topological defects induced by DHU. Since the observed DHU in 2D silica is associated with the local topological and geometrical constraints common in many 2D materials, we would expect to observe DHU and thus, the metallic behavior, in the amorphous states of other 2D materials, should such states be metastable at least. With the increasing interest in 2D amorphous materials, we expect our methods of building realistic structural model of amorphous 2D material systems along

with large-scale DFT calculations to be applicable to a wide range of other 2D materials such as graphene [61] and molybdenum disulfide [62] in the amorphous form.

Acknowledgments We thank P. Y. Huang for helpful

discussion and sharing TEM images of amorphous silica. Y. Z. and H. N. thank Arizona State University (ASU) for the University Graduate Fellowship. L. L. and H.Z. thank the start-up funds from ASU. The DFT calculations have been done on the USTC HPC facilities.

-
- [1] S. Torquato and F. H. Stillinger, *Physical Review E* **68**, 041113 (2003).
- [2] C. E. Zachary and S. Torquato, *Journal of Statistical Mechanics: Theory and Experiment* **2009**, P12015 (2009).
- [3] A. Gabrielli, M. Joyce, and F. S. Labini, *Physical Review D* **65**, 083523 (2002).
- [4] A. Donev, F. H. Stillinger, and S. Torquato, *Physical review letters* **95**, 090604 (2005).
- [5] C. E. Zachary, Y. Jiao, and S. Torquato, *Physical review letters* **106**, 178001 (2011).
- [6] Y. Jiao and S. Torquato, *Physical Review E* **84**, 041309 (2011).
- [7] D. Chen, Y. Jiao, and S. Torquato, *The Journal of Physical Chemistry B* **118**, 7981 (2014).
- [8] C. E. Zachary and S. Torquato, *Physical Review E* **83**, 051133 (2011).
- [9] S. Torquato, G. Zhang, and F. Stillinger, *Physical Review X* **5**, 021020 (2015).
- [10] O. U. Uche, F. H. Stillinger, and S. Torquato, *Physical Review E* **70**, 046122 (2004).
- [11] R. D. Batten, F. H. Stillinger, and S. Torquato, *Journal of Applied Physics* **104**, 033504 (2008).
- [12] R. D. Batten, F. H. Stillinger, and S. Torquato, *Physical review letters* **103**, 050602 (2009).
- [13] J. L. Lebowitz, *Physical Review A* **27**, 1491 (1983).
- [14] G. Zhang, F. H. Stillinger, and S. Torquato, *Physical Review E* **92**, 022119 (2015).
- [15] G. Zhang, F. H. Stillinger, and S. Torquato, *Physical Review E* **92**, 022120 (2015).
- [16] L. Berthier, P. Chaudhuri, C. Coulais, O. Dauchot, and P. Sollich, *Physical review letters* **106**, 120601 (2011).
- [17] R. Kurita and E. R. Weeks, *Physical Review E* **84**, 030401 (2011).
- [18] G. L. Hunter and E. R. Weeks, *Reports on progress in physics* **75**, 066501 (2012).
- [19] R. Dreyfus, Y. Xu, T. Still, L. A. Hough, A. Yodh, and S. Torquato, *Physical Review E* **91**, 012302 (2015).
- [20] D. Hexner and D. Levine, *Physical review letters* **114**, 110602 (2015).
- [21] R. L. Jack, I. R. Thompson, and P. Sollich, *Physical review letters* **114**, 060601 (2015).
- [22] J. H. Weijs, R. Jeanneret, R. Dreyfus, and D. Bartolo, *Physical review letters* **115**, 108301 (2015).
- [23] E. Tjhung and L. Berthier, *Physical review letters* **114**, 148301 (2015).
- [24] S. Torquato, A. Scardicchio, and C. E. Zachary, *Journal of Statistical Mechanics: Theory and Experiment* **2008**, P11019 (2008).
- [25] R. Feynman and M. Cohen, *Physical Review* **102**, 1189 (1956).
- [26] Y. Jiao, T. Lau, H. Hatzikirou, M. Meyer-Hermann, J. C. Corbo, and S. Torquato, *Physical Review E* **89**, 022721 (2014).
- [27] A. Mayer, V. Balasubramanian, T. Mora, and A. M. Walczak, *Proceedings of the National Academy of Sciences* **112**, 5950 (2015).
- [28] M. Hejna, P. J. Steinhardt, and S. Torquato, *Physical Review B* **87**, 245204 (2013).
- [29] R. Xie, G. G. Long, S. J. Weigand, S. C. Moss, T. Carvalho, S. Roorda, M. Hejna, S. Torquato, and P. J. Steinhardt, *Proceedings of the National Academy of Sciences* **110**, 13250 (2013).
- [30] M. A. Klatt, J. Lovrić, D. Chen, S. C. Kapfer, F. M. Schaller, P. W. Schönhofer, B. S. Gardiner, A.-S. Smith, G. E. Schröder-Turk, and S. Torquato, *Nature communications* **10**, 811 (2019).
- [31] D. Hexner and D. Levine, *Physical review letters* **118**, 020601 (2017).
- [32] D. Hexner, P. M. Chaikin, and D. Levine, *Proceedings of the National Academy of Sciences* **114**, 4294 (2017).
- [33] J. H. Weijs and D. Bartolo, *Physical review letters* **119**, 048002 (2017).
- [34] Q.-L. Lei, M. P. Ciamarra, and R. Ni, *Science advances* **5**, eaau7423 (2019).
- [35] Q. Lei and R. Ni, *arXiv preprint arXiv:1904.07514* (2019).
- [36] S. Torquato, G. Zhang, and M. De Courcy-Ireland, *Journal of Physics A: Mathematical and Theoretical* **52**, 135002 (2019).
- [37] M. Florescu, S. Torquato, and P. J. Steinhardt, *Proceedings of the National Academy of Sciences* **106**, 20658 (2009).
- [38] W. Man, M. Florescu, K. Matsuyama, P. Yadak, G. Nahal, S. Hashemizad, E. Williamson, P. Steinhardt, S. Torquato, and P. Chaikin, *Optics express* **21**, 19972 (2013).
- [39] W. Man, M. Florescu, E. P. Williamson, Y. He, S. R. Hashemizad, B. Y. Leung, D. R. Liner, S. Torquato, P. M. Chaikin, and P. J. Steinhardt, *Proceedings of the National Academy of Sciences* **110**, 15886 (2013).
- [40] G. Zhang, F. Stillinger, and S. Torquato, *The Journal of chemical physics* **145**, 244109 (2016).
- [41] Y. Xu, S. Chen, P.-E. Chen, W. Xu, and Y. Jiao, *Physical Review E* **96**, 043301 (2017).
- [42] S. Torquato and D. Chen, *Multifunctional Materials* **1**, 015001 (2018).
- [43] J. Haberko, N. Muller, and F. Scheffold, *Physical Review A* **88**, 043822 (2013).
- [44] G. Zito, G. Rusciano, G. Pesce, A. Malafrente, R. Di Girolamo, G. Ausanio, A. Vecchione, and A. Sasso, *Physical Review E* **92**, 050601 (2015).
- [45] K. Binder and W. Kob, *Glassy materials and disordered solids: An introduction to their statistical mechanics* (World scientific, 2011).
- [46] P. Y. Huang, S. Kurasch, J. S. Alden, A. Shekhawat, A. A. Alemi, P. L. McEuen, J. P. Sethna, U. Kaiser, and D. A. Muller, *science* **342**, 224 (2013).
- [47] Z. Ma and S. Torquato, *Journal of Applied Physics* **121**,

- 244904 (2017).
- [48] S. Munetoh, T. Motooka, K. Moriguchi, and A. Shintani, *Computational Materials Science* **39**, 334 (2007).
- [49] S. Plimpton, *Journal of computational physics* **117**, 1 (1995).
- [50] A. J. Stone and D. J. Wales, *Chemical Physics Letters* **128**, 501 (1986).
- [51] J. P. Perdew, K. Burke, and M. Ernzerhof, *Phys. Rev. Lett.* **77**, 3865 (1996).
- [52] Z. Gao, X. Dong, N. Li, and J. Ren, *Nano letters* **17**, 772 (2017).
- [53] P. Y. Huang, S. Kurasch, A. Srivastava, V. Skakalova, J. Kotakoski, A. V. Krasheninnikov, R. Hovden, Q. Mao, J. C. Meyer, J. Smet, et al., *Nano letters* **12**, 1081 (2012).
- [54] M. Chen, G. Guo, and L. He, *Journal of Physics: Condensed Matter* **22**, 445501 (2010).
- [55] P. Li, X. Liu, M. Chen, P. Lin, X. Ren, L. Lin, C. Yang, and L. He, *Computational Materials Science* **112**, 503 (2016).
- [56] The electronic structure calculations are computed by Atomic-orbital Based Ab-initio Computation at UStc (ABACUS) with numerical atomic orbitals. We adopt the PBE functional and pseudopotential and use double-zeta plus polarisation (DZP) basis sets (Si: $2s2p1d$, O: $2s2p1d$), the cutoffs for Si and O orbitals are set to 8 and 7 a.u., respectively. The energy cutoff is set to 100 Ry. A single k-point (Γ point) is used for the two large supercells each containing 1800 atoms.
- [57] E. Gao, B. Xie, and Z. Xu, *Journal of Applied Physics* **119**, 014301 (2016).
- [58] L. Yang, K. Majumdar, H. Liu, Y. Du, H. Wu, M. Hatzistergos, P. Hung, R. Tieckelmann, W. Tsai, C. Hobbs, et al., *Nano letters* **14**, 6275 (2014).
- [59] B. Kramer and A. MacKinnon, *Reports on Progress in Physics* **56**, 1469 (1993).
- [60] P. W. Anderson, *Physical review* **109**, 1492 (1958).
- [61] D. Van Tuan, A. Kumar, S. Roche, F. Ortmann, M. Thorpe, and P. Ordejon, *Physical Review B* **86**, 121408 (2012).
- [62] X. Zhang, Y. Zhang, B.-B. Yu, X.-L. Yin, W.-J. Jiang, Y. Jiang, J.-S. Hu, and L.-J. Wan, *Journal of Materials Chemistry A* **3**, 19277 (2015).

Supplemental Material: Enhanced Electronic Transport in Disordered Hyperuniform Two-Dimensional Amorphous Silica

Yu Zheng*,¹ Lei Liu*,² Hanqing Nan*,² Zhen-Xiong Shen*,^{3,4} Ge Zhang,⁵ Duyu Chen,⁶ Lixin He,^{3,4} Wenxiang Xu,^{7,2,†} Mohan Chen,^{8,‡} Yang Jiao,^{2,1,§} and Houlong Zhuang^{2,¶}

¹*Department of Physics, Arizona State University, Tempe, AZ 85287*

²*Materials Science and Engineering, Arizona State University, Tempe, AZ 85287*

³*Key Laboratory of Quantum Information, University of Science and Technology of China, Hefei, Anhui 230026, P. R. China*

⁴*Synergetic Innovation Center of Quantum Information and Quantum Physics, University of Science and Technology of China, Hefei, Anhui 230026, P. R. China*

⁵*Department of Physics, University of Pennsylvania, Philadelphia, PA 19104*

⁶*Tepper School of Business, Carnegie Mellon University, Pittsburgh, PA 15213*

⁷*College of Mechanics and Materials, Hohai University, Nanjing 211100, P.R. China*

⁸*CAPT, HEDPS, College of Engineering, Peking University 100871, P.R. China*

EXPERIMENTAL PROCEDURE FOR FABRICATING 2D AMORPHOUS SILICA SAMPLES

The 2D amorphous silica samples analyzed in paper were fabricated using a low-pressure chemical vapor deposition (CVD) technique which has been described in detail in Refs. [46] and [53] of the paper. In particular, the amorphous silica supported by graphene was grown on polycrystalline Cu foils attached to a quartz substrate using a low-pressure CVD technique with hexane being the precursor. The growth occurred in a quartz tube following four steps. First, the pressure in the tube was pumped down close to zero (10^{-2} mbar). Second, a formation gas (Ar/(5%)H₂) with a pressure of about 5 mbar was introduced to the tube. Meanwhile, the Cu foils were heated to a high temperature (950 °C); Third, the hexane gas with a pressure of 0.5 mbar was also introduced to the tube for 1 minute. Finally, the temperature in the tube was lowered to room temperature while the formation gas kept flowing. We show via simulations that the observed DHU in amorphous silica is closely related to the strong topological and geometrical constraints induced by the local chemical order in the system. In addition, our density functional theory calculations show that DHU significantly reduces the electronic band gap in 2D amorphous silica, leading to almost complete closure of the band gap compared to the crystalline counterpart. This is in contrast to the conventional wisdom that disorder generally diminishes electronic transport and is due to the unique electron wave localization induced by DHU.

It was proposed in Ref. [53] that, air leaked to the tube caused the oxidized Cu surfaces, which further reacted with the quartz substrate, leading to the formation of the amorphous silica. The material samples were further characterized and imaged using transmission electron microscope (TEM). We analyzed the TEM images

of the amorphous silica samples obtained from these experimental conditions (see Fig. S1). We found that all of the samples exhibit the DHU feature. Our results suggest that DHU might be an intrinsic structural feature for all amorphous 2D materials, due to the strong topological and geometrical constraints induced by local chemical orders in these systems.

SPECTRAL DENSITY ANALYSIS AND HYPERUNIFORMITY

In the main paper, we provided the spectral density analysis of the experimental 2D amorphous silica and the numerical model, which show excellent agreement with one another. Here, we perform a scaling analysis of the small- k behavior of the spectral density $\psi(k)$ and analysis of hyperuniformity in the infinite-system limit (zero-wavenumber limit).

Fig. S2 shows the spectral density $\psi(k)$ at small wavenumbers in log-log plot for the experimental system (left panel) and numerical model (right panel). The data was fitted using linear regression, and the slope for the experimental system and numerical model is 1.021 and 1.079, respectively. These results indicate that the spectral density scales linearly with k for both systems, i.e., $\psi(k) \propto k$. Similar scaling behaviors have also been observed in disordered jammed packing of hard particles and photoreceptor distributions in avian retina [1, 2].

To ascertain hyperuniformity of the system in the thermodynamic limit, we carry out a scaling analysis of zero-wavenumber limit of the spectral density $\psi(k \rightarrow 0)$ estimated from finite systems. In particular, for a given finite system size L , we first estimate $\psi(k \rightarrow 0; L)$ by employing a 3rd order polynomial fitting, i.e., $\psi(k; L) \approx a_0(L) + a_1(L)k + a_2(L)k^2 + a_3(L)k^3$ for small k values, where the coefficient $a_0(L)$ provides an estimate of $\psi(k \rightarrow 0; L)$. Fig. S3 shows the estimated $\psi(k \rightarrow 0; L)$ as a function of system size $1/L$, obtained from the numerical system. The analysis shows that $\psi(k \rightarrow 0; L)$ is clearly a monotonic decreasing function of L and

*These authors contributed equally to this work.

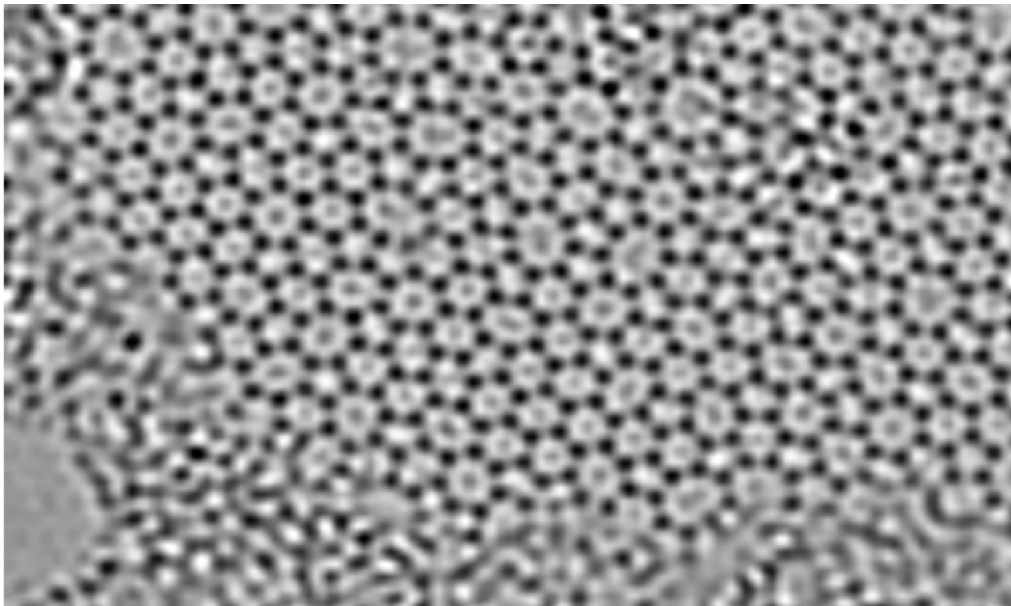


FIG. S1: TEM image of a typical 2D amorphous silica sample.

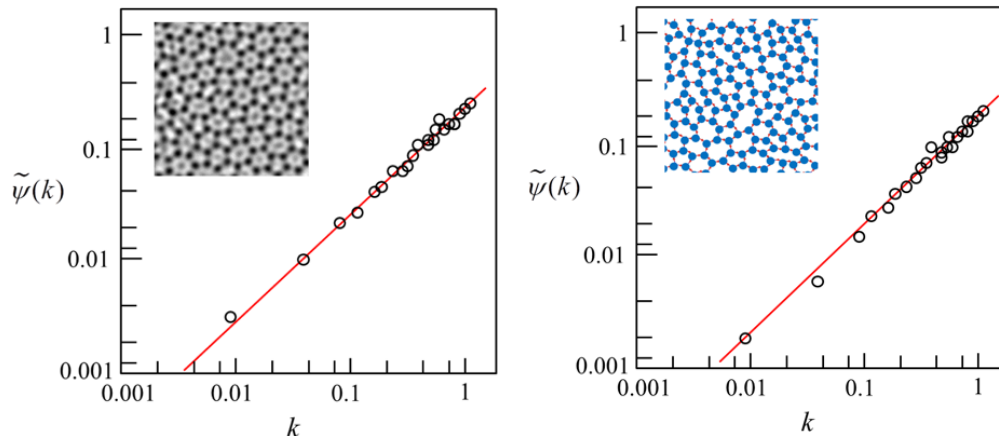


FIG. S2: Spectral density $\psi(k)$ at small wavenumbers in log-log plot for the experimental system (left panel) and numerical model (right panel), which indicates that spectral density scales linearly with k for both systems.

$\psi(k \rightarrow 0; L \rightarrow \infty) \rightarrow 0$, which indicates the system is hyperuniform in the thermodynamic limit. We note that due to the limited field of view of the TEM, we were not able to carry out a similar scaling analysis based on the experimental data. However, since the numerical model is structurally representative of the actual system on different length scales and topologically, we expect the actual 2D amorphous silica is also hyperuniform in the thermodynamic limit. Finally, we note that increasing system size does not affect the linear scaling behavior for small wavenumbers.

COMPARISON OF STRUCTURAL STATISTICS OF EXPERIMENTAL SYSTEM AND NUMERICAL MODELS

In the main paper, we show that spectral density and ring statistics of the experimental system and numerical model agree very well with one another, indicating the model is structurally representative of the 2D amorphous silica on large length scales and topologically. Here, we compute and compare local structural statistics of the experimental and numerical systems, including the pair-correlation function $g_2(r)$ and the nearest-neighbor distribution $P(r)$ associated with the Si atoms, which are shown in Fig. S5 and Fig. S6, respectively.

It can be seen again that these statistics agree well with

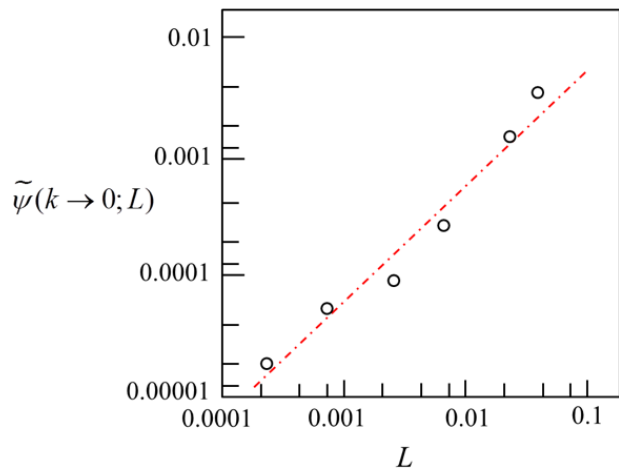


FIG. S3: Extrapolation of the zero-wavenumber limit of the spectral density in the infinite-system limit (i.e., the thermodynamic limit) based on the numerical results.

This scaling analysis indicates the system remains hyperuniform in the thermodynamic limit.

one another. In particular, the $g_2(r)$ possesses an exclusion volume region, an average coordination number (the value of first peak) of 3 and quickly decays to unity, indicating no long-range order in the system. The $P(r)$ functions show narrow distributions, indicating small variations in the bond lengths. These results indicate that the local chemical order (i.e., Si-O bonds) induces strong local topological and geometrical constraints that are closely related to the observed disordered hyperuniformity in the system.

HIGH-ENERGY STATES IN AMORPHOUS SILICA

STONE-WALES TRANSFORMATIONS PRESERVE HYPERUNIFORMITY

In the main text, we provide an argument for the emergence of hyperuniformity in the amorphous 2D silica, i.e.,

the Stone-Wales transformations, which only induce local topological perturbations in the system, preserve hyperuniformity. In this section, we provide numerical evidence for this argument.

In particular, we first generate a perfect honeycomb lattice packing of Si atoms (containing ~ 1000 atoms), with the lattice vectors consistent with those defining the crystalline SiO₂ structure. Next, we gradually introduce Stone-Wales defects in the system, by flipping randomly selected bonds, with constraints that a bond can be flipped only once. We define the concentration of the Stone-Wales defects as the number bonds affected by the Stone-Wales transformation over the total number of bonds in the system. The insets of Fig. S8 show typical configurations with different defect concentrations. Next, we compute the spectral density of the configurations containing different concentrations of Stone-Wales defects, which are shown in Fig. S8. It can be clearly seen that for all concentrations we study (from 0% to 75%), the systems all remain hyperuniform, which indicates Stone-Wales transformations preserve hyperuniformity.

[†] correspondence sent to: xwxfat@gmail.com

[‡] correspondence sent to: mohanchen@pku.edu.cn

[§] correspondence sent to: yang.jiao.2@asu.edu

[¶] correspondence sent to: hzhuang7@asu.edu

- [1] Y. Jiao, T. Lau, H. Hatzikirou, M. Meyer-Hermann, J. C. Corbo, and S. Torquato, *Physical Review E* **89**, 022721 (2014).
- [2] R. Dreyfus, Y. Xu, T. Still, L. A. Hough, A. Yodh, and S. Torquato, *Physical Review E* **91**, 012302 (2015).

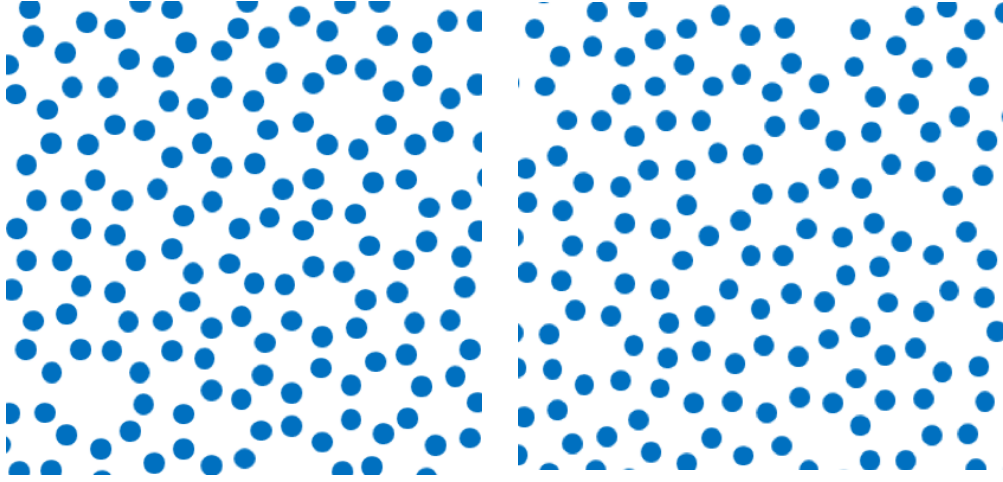


FIG. S4: Point configurations associated with the Si atoms derived based on the TEM images (left) and numerical network model (right). The two systems are visually very similar to one another.

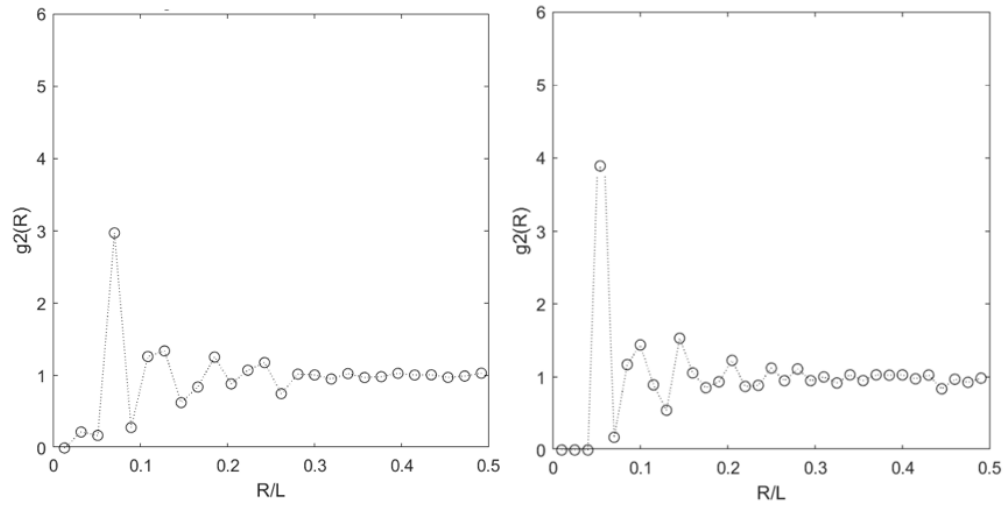


FIG. S5: Pair-correlation function $g_2(r)$ associated with the Si atoms of the experimental system (left) and numerical network model (right).

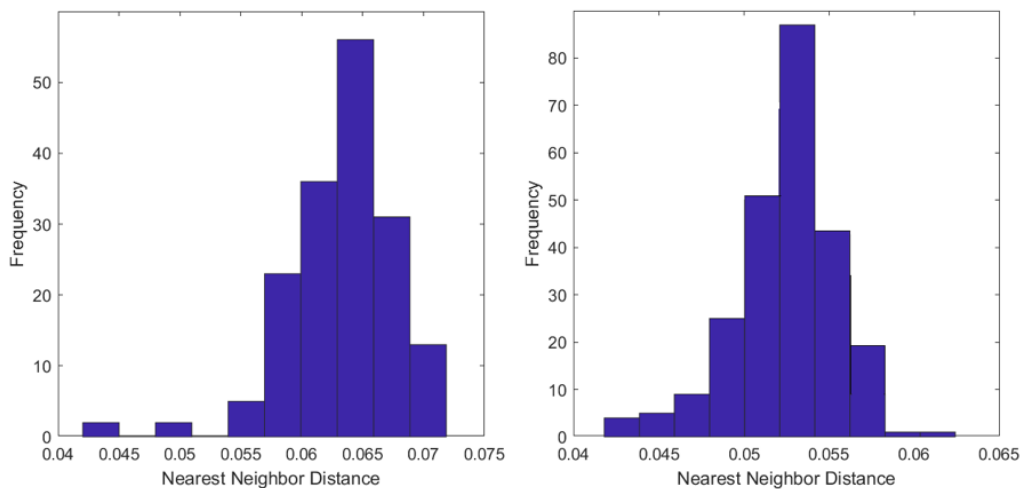


FIG. S6: Nearest-neighbor distribution $P(r)$ associated with the Si atoms of the experimental system (left) and numerical network model (right).

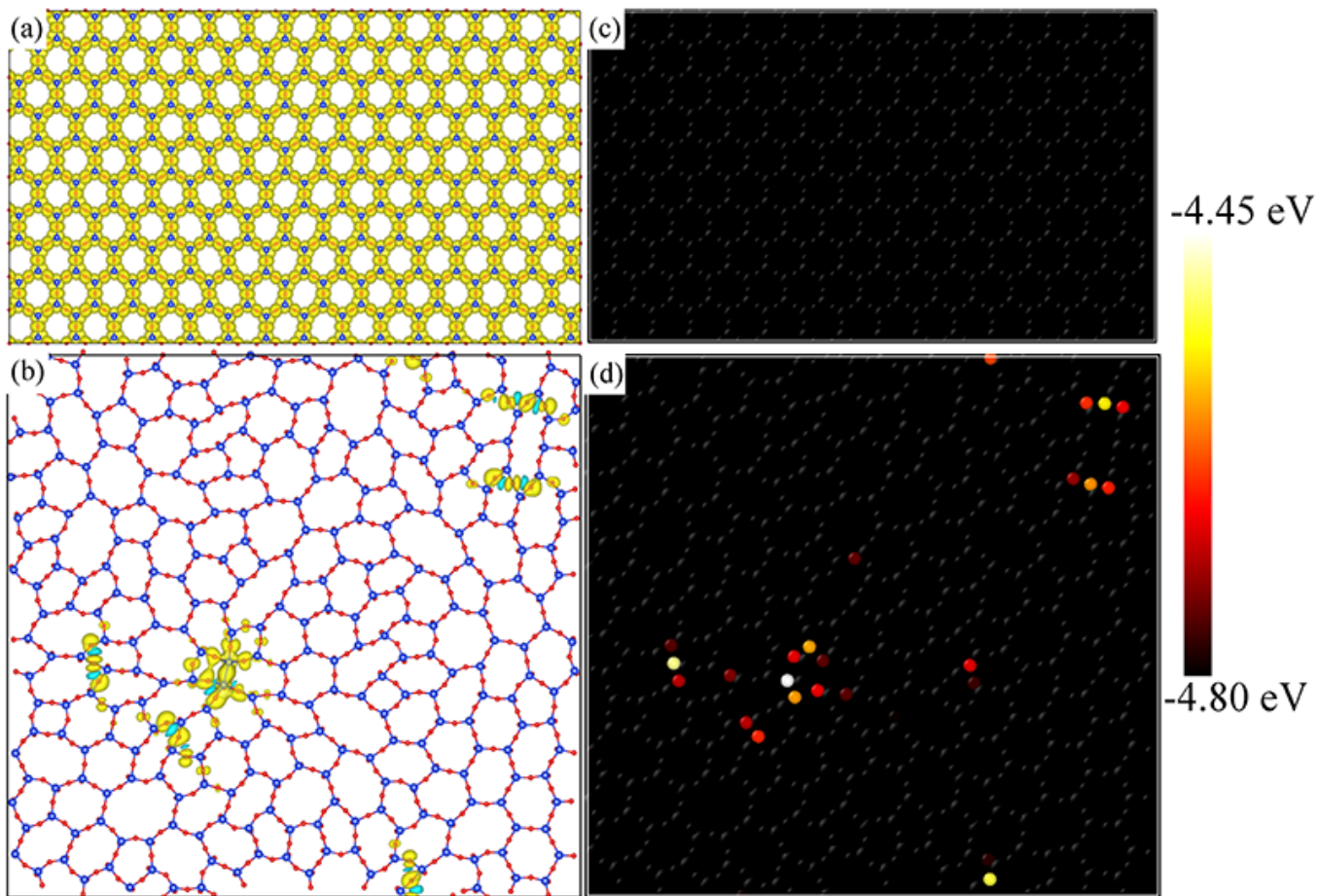


FIG. S7: Electron densities at the HOMO level of (a) the crystalline structure and (b) at the Fermi level of the DHU structure. The iso-surface value is $0.0023 \times 10^{-8} e/\text{Bohr}^3$. The corresponding distributions of potential energies are shown in (c) and (d), respectively. The color bar shows a range of the distributions. A larger field of view for both systems are shown here than in the main text.

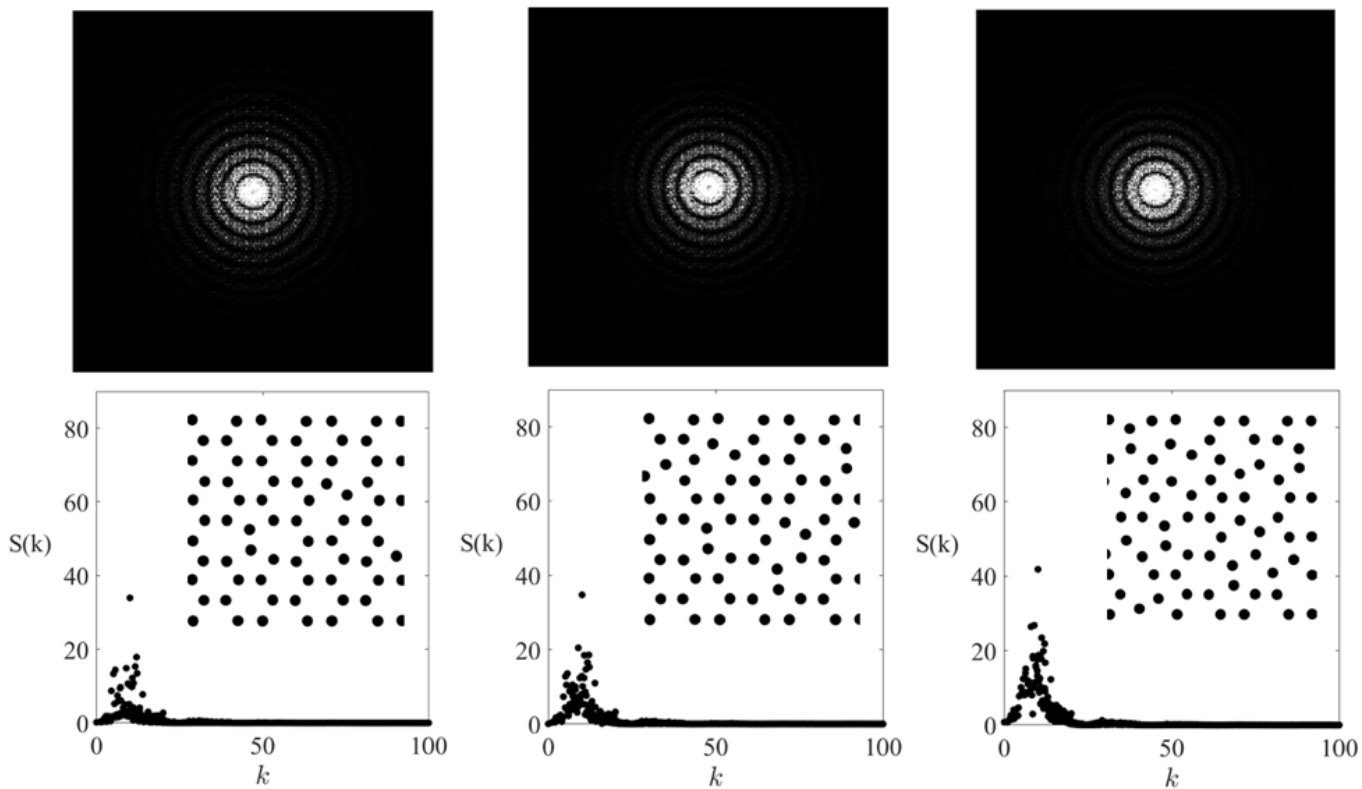


FIG. S8: Stone-Wales transformations preserve hyperuniformity. The figure shows the full spectral density (upper panels) and angular averaged spectral density (lower panels) for 2D distributions of Si atoms generated by random introducing different numbers of Stone-Wales defects. The concentration of the defects (see the text below for definition) is respectively 15%, 45%, and 70% for the left, middle and right figures (see insets for configurations of Si atoms). It can be clearly seen that for all cases the systems remain hyperuniform, which indicates Stone-Wales transformations preserve hyperuniformity.